ISSN 0015-4628, Fluid Dynamics, 2016, Vol. 51, No. 1, pp. 70–80. © Pleiades Publishing, Ltd., 2016.
Original Russian Text © M.A. Pakhomov, V.I. Terekhov, 2016, published in Izvestiya Rossiiskoi Akademii Nauk, Mekhanika Zhidkosti i Gaza, 2016, Vol. 51, No. 1, pp. 69–78.

Structure of the Nonisothermal Swirling Gas-Droplet Flow behind an Abrupt Tube Expansion

M. A. Pakhomov and V. I. Terekhov

Kutateladze Institute of Thermophysics, Siberian Branch, Russian Academy of Science, pr. Akademika Lavrent'eva 1, Novosibirsk, 630090 Russia

e-mail: pakhomov@ngs.ru, terekhov@itp.nsc.ru

Received April 2, 2015

Abstract—Flow structure and heat and mass transfer in a swirling two-phase stream is numerically modeled using the Reynolds stress transport model. The gas phase is described by the 3D RANS system of equations with account for the inverse influence of particles on the transport processes in the gas. The gas phase turbulence is calculated using the Reynolds stress transport model with account for the presence of disperse particles. The two-phase nonswirling flow behind an abrupt tube expansion contains a secondary corner vortex which is absent from the swirling flow. The disperse phase is redistributed over the tube cross-section. Large particles are concentrated in the wall region of the channel under the action of the centrifugal forces, while the smaller particles are in the central zone of the chamber.

Keywords: gas-droplet flow, separation, swirl, evaporation, numerical modeling, turbulence, Reynolds stress transport model.

DOI: 10.1134/S0015462816010087

Swirling gas-droplet flows in the presence of an abrupt expansion of a channel are widely used for stabilizing combustion in industrial burners and separators. The swirling flows are characterized by large local gradients of mean and fluctuation velocities and other parameters and are accompanied by complex hydrodynamic phenomena due to the action of the centrifugal and Coriolis forces [1–4]. The presence of recirculation flows has a considerable effect on the momentum and heat transfer intensity and particle or droplet dispersion, thus determining the structure of the turbulent two-phase flow [5–10]. The interaction between fine particles and turbulent eddies of the gas phase is a complicated and as yet not clearly understood process. For this reason, despite the wide practical application of two-phase flows, the turbulent transport in these media remains poorly studied.

In the literature there are a few studies devoted to experimental [11, 12] and numerical [12–16] investigation of swirling flows of the mixture of the air with solid particles. Free two-phase swirling jet flows [13] and flows behind an abrupt expansion of a tube [11, 12, 14–16] were studied. An investigation of these flows using the RANS equations was carried out in [12–15]. The Lagrangian [12, 14, 15] and Eulerian [13] approaches to the description of the disperse phase dynamics were applied. In [12–15] the gas phase turbulence is described using the k–ε model modified to cover the case of the presence of particles.

An experimental and numerical investigation of swirling gas-droplet flows behind an abrupt tube or channel expansion was carried out in [17–22]. The combustion of liquid fuel droplets was numerically simulated in [18–20]. In [18] the results of the numerical simulation on the basis of the Eulerian approach were compared with the authors' experimental data on the atomized fuel droplet evaporation in a swirling flow. The gas phase turbulence was described using the k–ε model taking account for the effects of the particles and the carrying flow swirl. Good agreement with the measured data was obtained, which counts in favor of the model developed in calculating the atomized fuel burning in combustion chambers. In [9]

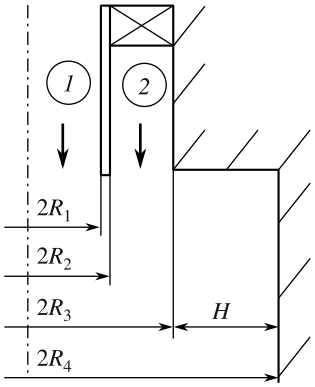

Fig. 1. Schematics of the computation domain; (*1*) gas-droplet, swirl-free flow and (*2*) single-phase swirling air flow.

swirling gas-droplet flow in a tube was modeled using the RANS approach with account for the burning of liquid fuel droplets. The gas turbulence effect on the droplet evaporation rate was shown. This effect cannot be neglected far from the inlet section at the swirl parameters $S < 1$ and near the section, where the swirling begins, at $S > 1$.

In the last decade large eddy simulation (LES) is increasingly more frequently used for modeling this kind of flows [16, 20–22]. This method makes it possible to calculate complicated processes occurring in two-phase flows under the conditions similar with those in actual combustors. However, the LES application, particularly with account for the disperse phase effect on subgrid stresses, requires high-performance supercomputers which restricts the application of this technique in engineering calculations of swirling two-phase flows in the presence of separation zones.

The dynamics of the fuel droplet propagation and the heat and mass transfer were investigated using LES in [20]. The droplet dynamics and their heat and mass exchange with the gas phase were calculated within the framework of the Lagrangian approach. It was shown that an increase in the swirl parameter leads to an increase in the particle dispersion degree over the combustor cross-section and the vortex breakdown. In two-phase flows combustion processes reduce the recirculation region length. The calculation of a swirling gas-droplet flow behind an abrupt expansion of a plane channel was carried out in [22] on the basis of the Eulerian and Lagrangian approaches. The calculations did not show any advantage of one method over another, as concerns both mean and fluctuation parameters of the two-phase flow.

One of the methods which makes it possible to partially allow for complicated mixing processes and the anisotropy of the phase velocity fluctuations in separated swirling single-phase flows is the use of the second moment closure (SMC) models [23, 24]. The agreement with the data of measurements was reasonable for both mean and fluctuating parameters. Some difficulties in describing these flows still remain; these are the incorrect negative sign of the *uw* correlation and the conservation of the vortical form of the tangential velocity component at large distances from the entrance at small values of the swirl parameter [23]. The successful SMC application in describing two-phase flows was shown in [10, 14, 25, 26].

The purpose of this study is to numerically model the swirl influence on the turbulent gas-droplet flow structure behind an abrupt expansion of a tube. The flow dynamics and heat and mass transfer in the gaseous and disperse phases are described using the Eulerian approach [26–28].

1. FORMULATION OF THE PROBLEM AND NUMERICAL MODEL

We consider the problem of the dynamics of a swirling turbulent two-phase gas-droplet flow in the presence of heat transfer to the channel walls. The solution is determined using the system of three-dimensional Reynolds-averaged Navier–Stokes equations (RANS) written with account for the inverse influence of the particles on the transport processes in the gas. The flow is schematically represented in Fig. 1. The volume

concentration of the disperse phase is small ($\Phi_1 = M_{L1}\rho/\rho_L < 2\times 10^{-4}$), while the particles are fairly fine ($d_1 < 100$ μm). For this reason, the effect of their collisions with each other can be neglected. Here, M_{L1} is the initial mass concentration of the droplets and ρ and ρ_L are the gas and droplet densities.

System of Averaged Equations for the Gas Phase

We will use the system of 3D RANS equations written in the cylindrical coordinates with account for the inverse influence of the particles on the processes of the mean and turbulent transfer in the gas

$$\rho\frac{\partial U_j}{\partial x_j} = \frac{6J}{d}\Phi,$$

$$\frac{\partial(U_iU_j)}{\partial x_i} = -\frac{1}{\rho}\frac{\partial(P + 2k/3)}{\partial x_i} + \frac{\partial}{\partial x_j}\left(\nu\frac{\partial U_j}{\partial x_j} - \langle u_iu_j\rangle\right)$$

$$- (U_i - U_{Li})\Phi\frac{\rho_L}{\rho}\left(\frac{1}{\tau} + \frac{6J}{\rho_L d}\right) + S_i,$$

$$\frac{\partial(U_iT)}{\partial x_i} = \frac{\partial}{\partial x_i}\left(\frac{\nu}{\mathrm{Pr}}\frac{\partial T}{\partial x_i} - \langle u_jT\rangle\right) + D_T\frac{(C_{PV} - C_{PA})}{C_P} \tag{1.1}$$

$$\times\left(\frac{\partial K_V}{\partial x_i}\frac{\partial T}{\partial x_i}\right) - \frac{6\Phi}{\rho C_P d}\left[\alpha(T - T_L) + JL\right],$$

$$\frac{\partial(U_iK_V)}{\partial x_i} = \frac{\partial}{\partial x_i}\left(\frac{\nu}{\mathrm{Sc}}\frac{\partial K_V}{\partial x_i} - \langle u_jK_V\rangle\right) + \frac{6J\Phi}{d},$$

$$\rho = P/(R_gT).$$

Here, the subscripts $i,\ j = 1, 2, 3$, U_i ($U_Z \equiv U$, $U_r \equiv V$, $U_\varphi \equiv W$) and u_i ($u_Z \equiv u$, $u_r \equiv v$, $u_\varphi \equiv w$) are the components of the mean velocity and of its fluctuations, $x_i(z,\ r,\ \varphi)$ are the axes of the cylindrical coordinates, ν is kinematic viscosity, $2k = \langle u_iu_i\rangle = u + v + w$ is the gas phase turbulence, J is the mass vapor flux from the surface of an evaporating droplet, P is the pressure, T is the temperature, D_T is the turbulent diffusion coefficient, C_P is the gas heat capacity, α is the coefficient of heat removal from an evaporating droplet, S_i is the flow swirl effect ($S_U = 0$, $S_V = W^2/r - vV/r^2 + w^2/r$, and $S_W = -VW/r - vW/r^2 + vw/r$) [23, 24], L is the specific heat of vaporization, K_V is the mass vapor concentration in the binary vapor-gas mixture, R_g is the specific gas constant, $\mathrm{Pr} = \nu/a$ and $\mathrm{Sc} = \nu/D$ are the Prandtl and Schmidt numbers, respectively, a is the coefficient of temperature conductivity, and D is the diffusion coefficient. The subscripts L, T, and V refer to the disperse phase, the turbulent parameters, and the water vapor, respectively.

All the equations of system (1.1) are written with account for the presence of disperse phase and the influence of its evaporation on the momentum, heat, and mass transfer in the gas flow. The turbulent heat and diffusion fluxes in the gas phase are defined in accordance with the Boussinesq hypothesis. The values of the turbulent Prandtl and Schmidt numbers were taken to be $\mathrm{Pr}_T = \mathrm{Sc}_T = 0.85$. The gas phase turbulence was calculated using the Reynolds stress transport model [29]. The redistributing term was written with account for the two-phase nature of the flow [30]. The inverse influence of the particles on the carrying phase turbulence was taken into account within the framework of the approach developed in [30]. The equations of the turbulence model [29] written with account for the two-phase nature of the flow can be found in [10, 26].

System of Averaged Equations for the Disperse Phase

The system of averaged equations governing the transport processes in the disperse medium are as follows:

$$\frac{\partial(\rho_L \Phi U_{Lj})}{\partial x_j} = -\frac{6J\Phi}{d},$$

$$\frac{\partial(\rho_L \Phi U_{Lj} U_{Li})}{\partial x_j} + \frac{\partial(\rho_L \Phi \langle u_{Li} u_{Lj} \rangle)}{\partial x_j}$$

$$= \Phi(U_i - U_{Li})\frac{\rho_L}{\tau} + \Phi\rho_L g - \frac{1}{\tau}\frac{\partial(\rho_L D_{Lij}\Phi)}{\partial x_j} - \frac{\partial(\Phi P)}{\partial x_i}, \tag{1.2}$$

$$\frac{\partial(\rho_L \Phi U_{Lj} T_{Li})}{\partial x_j} + \frac{\partial(\rho_L \Phi \langle \theta u_{Lj} \rangle)}{\partial x_j}$$

$$= \Phi(T_i - T_{Li})\frac{\rho_L}{\tau_\Theta} - \frac{1}{\tau_\Theta}\frac{\partial(\rho_L D^\Theta_{Lij}\Phi)}{\partial x_j}.$$

Here, D_{Lij} and D^Θ_{Lij} are the tensors of turbulent diffusion and turbulent heat transfer of the particles [31, 32], $\tau_\Theta = C_{PL}\rho_L d^2/(12\lambda Y)$ is the time of thermal relaxation of the droplets, $Y = (1 + 0.3\mathrm{Re}_L^{1/2}\mathrm{Pr}^{1/3})$, $\mathrm{Re}_L = |\mathbf{U} - \mathbf{U}_L| d/\nu$ is the disperse phase Reynolds number based on the interphase velocity, and ν is kinematic viscosity of the gas phase.

The equations for the second moments of the fluctuations of the velocity $\langle u_{Li} u_{Lj} \rangle$, the droplet temperature $\langle \theta_L^2 \rangle$, and the turbulent heat flux of the disperse phase $\langle \theta_L u_{Lj} \rangle$ are presented in [31, 32]. System (1.1), (1.2) is supplemented with the heat transfer equation at the interface under the condition of the temperature constancy along the droplet radius and the vapor mass conservation equation on the evaporating surface [26].

2. NUMERICAL SOLUTION

The technique of the numerical realization of the Eulerian approach is described in more detail in [10, 26]. The Reynolds stress components were determined in accordance with the approach developed in [33]. All the calculations were carried out on a grid consisting of $256 \times 80 \times 80 \approx 1.64 \times 10^6$ control volumes. The further increase in their number has only a slight effect on the results of the numerical calculations.

On the tube axis the conditions of smooth matching for both phases are preassigned, while the impermeability and no-slip conditions for the gas phase are imposed on the wall. The absorbing wall conditions [32] on the wall are used for the disperse phase, when a droplet that has hit the wall does not return into the flow. In the exit section the derivatives of all the unknown parameters in the axial direction are let to be zero. The entry parameter distributions are preassigned using the preliminary calculations of single-phase flow in a $150R$-long tube, where R is the tube radius. Thus, in the entry section we have a fully hydrodynamically stabilized gas flow. the disperse phase is added in the flow in the entry section. For the disperse phase the unknown parameter distributions over the tube cross-section were uniform. The initial values of the radial mean velocities of the phases were determined using the relations of the solid rotation law [13]

$$V_1 = 4SU_1 r/R, \qquad V_{L1} = 4S_L U_{L1} r/R,$$

$$S = \int_0^{R_3} \rho U_1 W_1 r^2\, dr \Big/ R_3 \int_0^{R_3} \rho U_1^2 r\, dr, \qquad S_L = \int_0^{R_3} \rho_L U_{L1} W_{L1} r^2\, dr \Big/ R_3 \int_0^{R_3} \rho_L U_{L1}^2 r\, dr,$$

where S is the air flow swirl parameter and S_1 is the disperse phase flow swirl parameter.

In the first stage, the comparisons were performed for the single-phase swirling air flow in a tube with an abrupt expansion [34]. Good agreement between the calculated and measured data was obtained for both mean and fluctuation parameters (the difference was not greater than 10 to 15%), which provided the foundation for conducting the calculations of gas-droplet flows using the Reynolds stress transport model.

3. ANALYSIS OF THE RESULTS OF THE NUMERICAL MODELING

The swirling two-phase gas-droplet flow was studied in the downward flow regime behind an abrupt tube expansion. The computation domain is schematically presented in Fig. 1. The main jet of the mixture of the air and water droplets (*1*) is supplied into the central channel ($2R_1$). The swirling single-phase gas flow (*2*) arrives through the annular channel ($R_3 - R_2$). The computation domain geometry is as follows: $2R_1 =$ 20 mm, $2R_2 = 26$ mm, $2R_3 = 40$ mm, $2R_4 = 100$ mm, and the step height $H = 30$ mm. The computation domain length $X = 1$ m. The mass-average axial velocity of the main air jet $U_{m1} = 15$ m/s and its mass flow rate $G_1 = 22.6$ g/s. The mass flow rate of the air in the secondary annular jet $G_2 = 18$ g/s. The flow swirl parameter

$$S = \int_0^{R_3} \rho U_1 W_1 r^2\, dr R_3 \Big/ \left(\int_0^{R_3} \rho U_1^2 r\, dr \right) = 0 \div 1.$$

The gas-phase Reynolds number $\mathrm{Re} = U_{\infty 1} 2R_1/\nu = 2 \times 10^6$. The initial mean axial droplet velocity $U_{L1} = 12$ m/s. The initial water droplet diameter $d_1 = 10$ to 100 μm and their mass concentration $M_{L1} = 0$ to 0.1. The particle relaxation time $\tau = \rho_L d^2/(18\rho\nu W) = 0.3$ to 30 ms, where $W = 1 + \mathrm{Re}_L^{2/3}/6$. The wall temperature was constant along the whole length of the computation domain, $T_w = 373$ K. The gas and droplet temperature at the entry was 293 K.

The criterion characterizing the degree of the particle entrainment into the gas phase flow is the Stokes number in the mean motion $\mathrm{Stk} = \tau/\tau_f$, where τ_f is the turbulent temporal macroscale. According to the data of [16], it may be assumed that $\tau_f = X/U_{m1} \approx 67$ ms; then $\mathrm{Stk} = \rho_L d^2 \mathrm{Re}/(18W) = 0.004$ to 0.45, which indicates that the particles are well entrained into the turbulent gas flow. For forward separated flows behind abrupt expansions in a tube and a plane channel the following expression for τ_f is given in [5, 6]: $\tau_f = 5H/U_{m1}$. Then under the conditions of our calculations $\tau_f = 10$ ms and $\mathrm{Stk} = 0.03$ to 2.5.

The gas phase streamlines in the swirling gas-droplet flow behind the abrupt tube expansion are plotted in Fig. 2. The calculations of the swirl-free separated flow ($S = 0$) were performed for the same geometry and the same mass flows of the two-phase and single-phase flows as for the swirling gas-droplet flow. Two recirculation zones are formed in the swirling flows. One of these is located in the wall region of the tube and is due to flow separation and reattachment. The second zone is within the near-axial region of the channel which is due to the appearance of return currents in swirling flows, which is in agreement with the data of measurements [11] and calculations [12, 15, 16] for swirling two-phase flows.

The two-phase swirl-free flow behind an abrupt tube expansion [10, 26] contains a secondary corner vortex (Fig. 2a) which is absent from the swirling flow. In the wall region of the tube a recirculation region followed by the two-phase flow reattachment is formed due to the abrupt expansion of the cylindrical channel (Fig. 2b).

In Fig. 3 we have plotted the radial profiles of the mean axial (a), radial (b), and tangential (c) velocities of the phases in several cross-sections along the computation domain length. The continuous curves correspond to the gas phase (*1*) and the broken curves to the disperse phase (*2*). The zones of negative gas velocities can be observable in the wall and axial regions of the tube which confirms the data in Fig. 2. For the disperse phase the presence of negative velocities in the axial region of the tube is also noticeable which indicates the disperse phase entrainment into the turbulent gas flow. Clearly, the particles lag behind somewhat the gas phase at the expense of the inertia, in all sections except the first (Fig. 3a). All the calculated profiles of the axial velocity of the gas have an expected maximum, whose position is displaced toward the tube wall as we move downstream, except for the first section. The radial velocity component suffers complicated

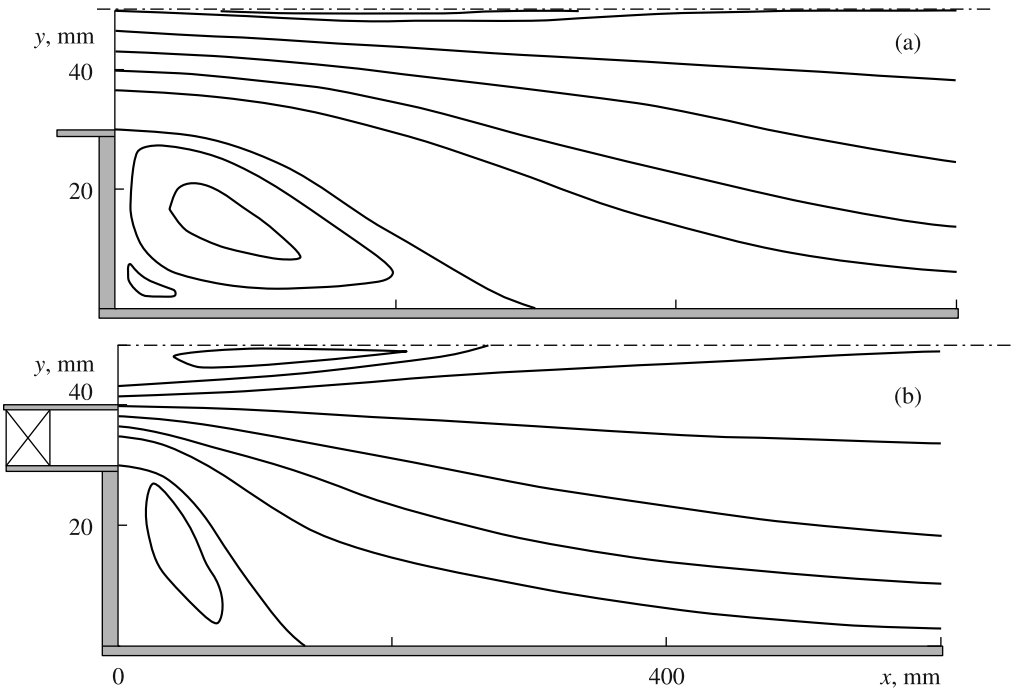

Fig. 2. Streamlines in the separated (a) and swirling (b) gas-droplet flows behind the abrupt tube expansion; $\mathrm{Re} = 2 \times 10^4$, $d_1 = 30$ μm, $\mathrm{Stk} = 0.3$, $M_{L1} = 0.05$, and $S = 0.5$.

variations within the chamber and is considerably reduced and equalized with respect to the cross-section near the exit section (Fig. 3b). The similar deformations are also inherent in the tangential velocities of the gas and the solid particles; in the exit sections they are similar in value and are restructured in accordance with the quasisolid rotation law (Fig. 3c).

4. COMPARISON WITH THE DATA OF MEASUREMENTS

Gas-Disperse Swirling Flow

In the first stage, the comparisons were made with the available experimental data for an isothermal swirling gas-disperse flow [11]. The swirling two-phase flow was studied in the downward flow regime behind an abrupt tube expansion. The experimental region geometry was as follows: $2R_1 = 32$ mm, $2R_2 = 38$ mm, $2R_3 = 64$ mm, and $2R_4 = 194$ mm. The step height $H = 65$ mm and the working section length $X = 1500$ mm. The main nonswirling jet of the mixture of a gas and glass particles enters through an axial orifice, while the swirling air flow is supplied through an annular orifice. The mass flow rate of the main gas jet $G_{A1} = 9.9$ g/s (supplied through the tube, $2R_1$ in diameter) and that of the secondary annular jet $G_{A2} = 38.3$ g/s (supplied through the annular slot $(R_3 - R_2)$). The flow swirl parameter $S = 0.47$. The Reynolds number $\mathrm{Re} = U_m 2R_3/\nu = 5.24 \times 10^4$, the mean initial air flow velocity $U_{m1} = 12.9$ m/s, the mean arithmetic diameter of the glass particles $d = 45$ μm, and their mass concentration $M_P = 0.034$. The air and solid particle temperature was 300 K. The measurement were carried out using the single-component phase Doppler anemometer (PDA).

The radial profiles of the measured [11] and calculated mass fluxes of the particles along the axial coordinate are plotted in Fig. 4. The mass flux was calculated from the formula $F = \rho_P U_P M_P$, where ρ_P, U_P, and M_P are the particle material density, their mean axial velocity, and the mass concentration, respectively. As we move away from the entry section, a considerable variation in the disperse phase mass flux profile in the tube cross-section can be observable. The mass flux profile has a maximum in the near-axial region of the tube which is conserved up to the distance $x = 195$ mm from the abrupt expansion. Starting from the second cross-section ($x = 112$ mm) the disperse phase is accumulated in the wall region of the cylindrical

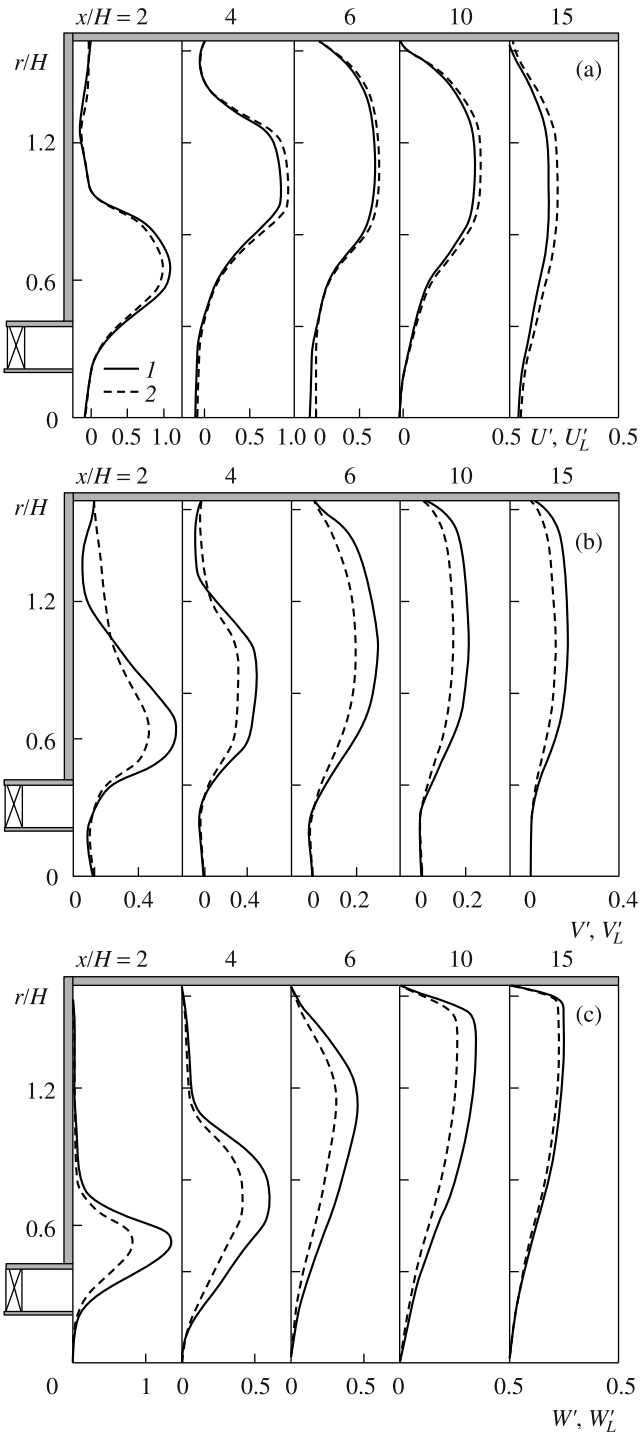

Fig. 3. Profiles of the mean axial $U' = U/U_{m1}$ and $U'_L = U_{L1}/U_{m1}$ (a), radial $V' = V/V_{m1}$ and $V'_L = V_{L1}/V_{m1}$ (b), and tangential $W' = W/W_{m1}$ and $W'_L = W_{L1}/W_{m1}$ (c) gas (*1*) and droplet (*2*) velocities in the swirling gas-droplet flow; parameters are the same as in Fig. 2.

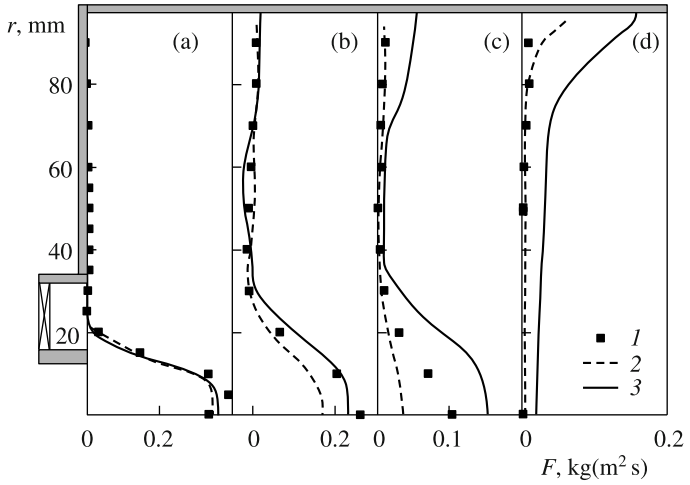

Fig. 4. Radial distributions of the particle mass flux in the swirling two-phase flow behind the abrupt tube expansion; (*1*) measurements [11]; (*2*) calculations [12]; and (*3*) calculations of this study; $d = 45$ μm, Stk $= 0.58$, $M_P = 0.034$, $S = 0.47$, and $x = 52$ (a), 112 (b), 195 (c), and 315 mm (d).

channel as a result of an increase in the tangential velocity of the particles and the turbophoresis force action which is in agreement with the results [11, 12]. Except from the axial zone, a good agreement with the data of measurements [11] can be noted. In the $x = 315$ mm section the experimental data are presented only for the wall region. Since, at the expense of the centrifugal forces, particles are ejected from the axial region toward the tube periphery, their number is insufficient for obtaining plausible data using the PDA method. In the $x = 52$, 112, and 195 mm sections the disperse phase concentration decreases more rapidly than it was noted in the experiments. Correspondingly, this leads to an increase in the particle number in the wall region of the channel.

Swirling Gas-Droplet Flow

To make comparisons in the case of swirling gas-droplet flows behind an abrupt tube expansion we used the results of the LES calculations [22] and the experiments [35]. The swirling two-phase flow of the mixture of air and kerosene droplets was studied in a horizontal channel behind an abrupt tube expansion. The height of the channel of square cross-section was 130 mm and its length was 245 mm. The step height $H = 50$ mm. The kerosene-supply nozzle diameter $2R_1 = 5$ mm and the diameter of the peripheral air-supply orifice $2R_3 = 30$ mm. The mass gas flow rate $G_A = 15$ g/s and that of the disperse phase $G_L = 1$ g/s. The flow swirl parameter $S = 0.7$. The mean initial air flow velocity $U_{m1} = 35$ m/s and the Reynolds number $\mathrm{Re} = U_m 2R_3/\nu = 7 \times 10^4$; the mean droplet diameter in [22] $d \approx 55$ μm. The thermal properties of kerosene are taken from [36]. The entry temperatures of the air and the kerosene droplets were $T_1 = 463$ K and $T_{L1} = 300$ K. The measurements were performed using the phase Doppler anemometer under the atmospheric pressure. As the entry distributions of the mean and fluctuation parameters of both phases, we took the experimental data [35] obtained at a distance $x = 6$ mm from the two-phase flow supply section. The initial mean size of monodisperse droplets was 50 μm. In the mean flow the Stokes number $\mathrm{Stk} = \tau/\tau_f = 0.6$, where $\tau_f = 5H/U_{m1} = 5$ ms. This indicates that the particles are well entrained into the turbulent gas flow [37, 38].

The profiles of the kerosene droplet diameter along the chamber section are presented in Fig. 5. Clearly that there is qualitative agreement with the measured data [35]. The disagreement with the LES calculation data [22] is considerable. Characteristic of these experiments is the particle dispersion over the plane channel cross-section. The larger particles are located in the wall region of the channel due to the centrifugal force action, while the finer ones are concentrated in the central recirculation zone of the chamber. The droplets that have found themselves in the axial separation zone cannot leave it, since the turbulence level in the

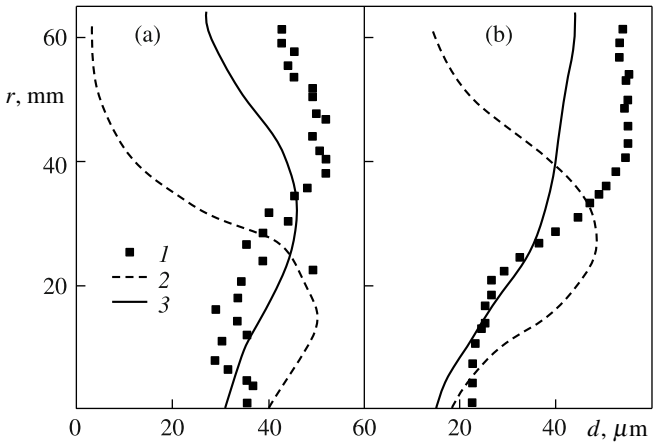

Fig. 5. Droplet diameter profiles in the swirling gas-droplet flow behind the abrupt expansion of the plane channel; (*1*) measurements [35]; (*2*) LES calculations [22]; and (*3*) calculations of this study; $d = 55$ μm, Stk $= 0.6$, $M_L = 0.034$, $S = 0.7$, and $x = 26$ (a) and 56 mm (b).

surrounding space is higher than that of the disperse phase, so that the recirculation region is the sort of a barrier for them. For this reason, the droplets that have found themselves in the central recirculation region are better heated and evaporated, which leads to a decrease in their dimensions.

Summary. A mathematical model of a swirling turbulent gas-droplet flow behind an abrupt tube expansion in the presence of disperse phase evaporation is developed and the numerical modeling is performed.

The two-phase swirl-free ($S = 0$) flow behind an abrupt tube expansion contains a secondary corner vortex which is absent from the swirling flow. In the swirling flow there are two recirculation zones: one is located in the axial region of the tube and is formed due to flow rotation, while the other is in the wall region of the channel. The reason for its formation is flow separation followed by its reattachment. Large particles are located in the wall region of the channel due to the centrifugal force action. The finer particles are concentrated in the central recirculation zone of the chamber. The droplets that have found themselves in the axial separation region cannot leave it, since in the shear layer the turbulence level is higher than that of the disperse phase.

The results obtained are compared with the data [11, 12, 22, 35] on the mean and fluctuation parameters of the swirling turbulent two-phase flow behind an abrupt tube expansion, including the case of droplet evaporation. The calculations are in reasonable agreement with the data of the measurements for swirling confined two-phase flows (the difference between the measured and calculated parameters is not greater than 20%). The efficiency of the mathematical model developed by the authors in the description of swirling two-phase flows behind an abrupt tube expansion is shown.

The study was carried out with the support of the Russian Science Foundation (project No. 14-19-00402).

REFERENCES

1. M.A. Gol'dshtik, *Vortex Flows* [in Russian], Nauka, Novosibirsk (1981).
2. S.S. Kutateladze, E.P. Volchkov, and V.I. Terekhov, *Aerodynamics and Heat and Mass Transfer in Confined Vortex Flows* [in Russian], Novosibirsk (1987).
3. A. Gupta, L. Lilley, and N. Syred, *Swirl Flows*, Abacus Press, Turnbridge Wells (1984).
4. A.A. Khalatov, *Theory and Practice of Swirling Flows* [in Russian], Naukova Dumka, Kiev (1989).
5. K. Hishida, T. Nagayasu, and M. Maeda, "Augmentation of Conductive Heat Transfer by an Effective Utilization of Droplet Inertia," Int. J. Heat Mass Transfer **38**, 1773 (1995).
6. J.B. Fessler and J.K. Eaton, "Turbulence Modification by Particles in a Backward-Facing Step Flow," J. Fluid Mech. **314**, 97 (1999).

7. E. Riber, V. Moureau, M. Garcia, T. Poinsot, and O. Simonin, "Evaluation of Numerical Strategies for Large Eddy Simulation of Particulate Two-Phase Recirculating Flows," J. Comp. Phys. **228**, 539 (2009).
8. F. Li, H. Qi, and C.F. You, "Phase Doppler Anemometry Measurements and Analysis of Turbulence Modulation in Dilute Gas-Solid Two-Phase Shear Flows," J. Fluid Mech. **663**, 434 (2010).
9. I. Senaha, Y. Miyafui, S. Kato, M. Higa, and M. Yaga, "Enhancement of Heat Transfer in the Downstream Region of a Backward-Facing Step Using a Small Amount of Mist (1st Report: Study of Heat Transfer Enhancement), (2nd report: Characteristics of Heat Transfer and Flow Behavior with Mist)," Trans. ASME. Pt. B **79**, 1816 (2013).
10. M.A. Pakhomov and V.I. Terekhov, "Numerical Investigation of Flow and Heat Transfer in a Gas-Droplet Separated Turbulent Stream Using the Reynolds Stress Transfer Model," Fluid Dynamics **48** (6), 789 (2013).
11. M. Sommerfeld and H.-H. Qiu, "Detailed Measurements in a Swirling Particulate Two-Phase Flow by a Phase-Doppler Anemometer," Int. J. Heat Fluid Flow **12**, 20 (1991).
12. M. Sommerfeld and H.-H. Qiu, "Characterization of Particle-Laden, Confined Swirling Flow by Phase-Doppler Anemometer and Numerical Calculation," Int. J. Multiphase Flow **19**, 1093 (1993).
13. A.A. Vinberg, L.I. Zaichik, and V.A. Pershukov, "Calculation of Two-Phase Swirling Flows," Fluid Dynamics **29** (1), 55 (1994).
14. L.X. Zhou, C.M. Liao, and T. Chen, "Simulation of Strongly Swirling Turbulent Gas-Particle Flows Using USM and k–ε–k_P Two-Phase Turbulence Models," Powder Techn. **114**, 1 (2001).
15. M. Seirjich and F. Menter, "Computation Grid Refinement in Modeling a Swirling Two-Phase Flow," Teplofiz. Aeromekh. **10**, 171 (2003).
16. S.V. Apte, K. Manesh, P. Moin, and J.C. Oefelein, "Large Eddy Simulation of Swirling Particle-Laden Flows in a Coaxial-Jet Combustor," Int. J. Multiphase Flow **29**, 1311 (2003).
17. L. Durdina, J. Jedelsky, and M. Jicha, "Investigation and Comparison of Spray Characteristics of Pressure-Swirl Atomizers for a Small-Sized Aircraft Turbine Engine," Int. J. Heat Mass Transfer **78**, 892 (2014).
18. G. Klose, R. Schmehl, R. Meier, G. Maier, R. Koch, S. Wittig, M. Hettel, W. Leuckel, and N.Zarzalis, "Evaluation of Advanced Two-Phase Flow and Combustion Models for Predicting Low Emission Combustors," ASME J. Gas Turbines Power **123**, 817 (2001).
19. A. Sadiki, M. Chrigui, J. Janicka, and M.R. Maneshkarimi, "Modeling and Simulation of Effects of Turbulence on Vaporization, Mixing and Combustion of Liquid-Fuel Sprays," Flow, Turbulence and Combustion **75**, 105 (2005).
20. V. Sankaran and S. Menon, "LES of Spray Combustion in Swirling Flows," J. Turbulence **3**, paper 011 (2002).
21. S. Apte, K. Mahesh, M. Gorokhovski, and P. Moin, "Stochastic Modeling of Atomizing Spray in a Complex Swirl Injector Using Large Eddy Simulation," Proc. Combustion Inst. **32**, 2257 (2009).
22. M. Sanjose, J.M. Senoner, F. Jaegle, B. Cuenot, S. Moreau, and T. Poisnot, "Fuel Injection Model for Euler–Euler and Euler–Lagrange Large-Eddy Simulation of an Evaporating Spray inside an Aeronautical Combustor," Int. J.Multiphase Flow **37**, 514 (2011).
23. S. Jakirlic, K. Hanjalic, and C. Tropea, "Modeling Rotating and Swirling Turbulence Flows: A Perpetual Challenge," AIAA J. **40**, 1984 (2002).
24. R. Jester-Zuerker, S. Jakirlic, and C. Tropea, "Computational Modeling of Turbulent Mixing in Confined Swirling Environment under Constant and Variable Density Conditions," Flow, Turbulence and Combustion **75**, 217 (2005).
25. M.A. Pakhomov and V.I. Terekhov, "Modeling of Turbulent Structure of an Upward Polydisperse Gas-Liquid Flow," Fluid Dynamics **50** (2), 229 (2015).
26. M.A. Pakhomov and V.I. Terekhov, "Second Moment Closure Modelling of Flow, Turbulence and Heat Transfer in Droplet-Laden Mist Flow in a Vertical Pipe with Sudden Expansion," Int. J.Heat Mass Transfer **66**, 210 (2013).
27. I.V. Dorevich and L.I. Zaichik, "Particle Deposition from a Turbulent Flow," Fluid Dynamics **23** (5), 722 (1988).
28. M.W. Reeks, "On a Kinetic Equation for the Transport of Particles in Turbulent Flows," Phys. Fluids A **3**, 446 (1991).
29. R. Manceau and K. Hanjalic, "Elliptic Blending Model: A New Near-Wall Reynolds-Stress Turbulence Closure," Phys. Fluids **14**, 744 (2002).
30. N. Beishuizen, B. Naud, and D. Roekaerts, "Evaluation of a Modified Reynolds-Stress Model for Turbulent Dispersed Two-Phase Flows Including Two-Way Coupling," Flow, Turbulence and Combustion **79**, 321 (2007).
31. L.I. Zaichik, "A Statistical Model of Particle Transport and Heat Transfer in Turbulent Shear Flows," Phys. Fluids **11**, 1521 (1999).
32. I.V. Derevich, "Statistical Modelling of Mass Transfer in Turbulent Two-Phase Dispersed Flows. 1. Model Development," Int. J. Heat Mass Transfer **43**, 3709 (2000).

33. K. Hanjalic and S. Jakirlic, "Contribution towards the Second-Moment Closure Modelling of Separating Turbulent Flows," Computers Fluids **27**, 137 (1998).
34. P.A. Dellenback, D.E. Metzger, and G.P. Neitzel, "Measurements in Turbulent Swirling Flow through an Abrupt Axisymmetric Expansion," AIAA J. **26**, 669 (1989).
35. N. Garcia-Rosa, "Phénomènes d'allumage d'un foyer de turbomachine en conditions de haute altitude," Ph. D. Thesis, Univ. de Toulouse, Institute Superieur de l'Aéronautique et de l'Espace, Toulose, France (2008).
36. K. Harstad and J. Bellan, "Modeling Evaporation of Jet a, JP-7, and RP-1 drops at 1 to 15 Bars," Combust. Flame **137**, 163 (2004).
37. A.Yu. Varaksin, "Hydrogasdynamics and Thermal Physics of Two-Phase Flows. Problems and Advances," Teplofiz. Vys. Temp. **51**, 421 (2013).
38. A.N. Osiptsov, "Mathematical Modeling of Dusty-Gas Boundary Layers," Appl. Math. Rev. **50**, 357 (1997).